Title: *In situ* analysis of mucus residing bacterial community reveals an ecological niche key for gut microbiome stability

Authors

Kellyanne Duncan[1], Kelly Carey-Ewend[1], and Shipra Vaishnava[1,2,*].

Affiliations:

[1]Molecular Microbiology and Immunology, Brown University, Providence, RI, 02912.

[2]Lead author

*Correspondence: Shipra Vaishnava (shipra_vaishnava@brown.edu)

Summary

Colonic mucus bacterial communities are critical for determining disease pathology and promoting colonization resistance. Yet the key ecological properties of mucus resident communities that make them crucial for maintaining homeostatic microbiome function remain poorly defined. Using an approach that combines *in situ* hybridization, laser microdissection and 16s rRNA sequencing of spatially distinct regions of the mouse gut lumen, we discovered that the microbial community embedded in the mucus layer is structurally and compositionally distinct and drives stability of the gut microbiome. Structurally, the mucus residing microbial community had a higher density of bacteria than in the lumen and formed a biofilm-like structure whose integrity was dependent on Gram-positive commensals. Compositionally the dense mucus community excluded bacteria belonging to phylum Proteobacteria. Additionally, the dense bacterial community in the mucus was significantly more diverse and consisted of bacterial species that were unique to it. Upon antibiotic treatment, the species-rich and dense bacterial community in the mucus lost fewer Firmicutes and showed smaller bloom of Proteobacteria compared to the lumen. Taken together our work discloses a crucial role for the mucus layer in promoting stability of the gut microbiome in the perfused intestinal ecosystem by spatially entrenching unique and diverse bacterial species.

Introduction

The past two decades have been a golden age for microbiome research. Exhaustive efforts to characterize the human and experimental animal microbiome coupled with exciting advances in sequencing technologies and computational techniques have immensely enhanced our knowledge about the diversity of the host-associated microbiome. By comparing microbial composition between different physiologic states it has become clear that various aspects of host physiology, metabolism, and immune system are intimately linked to the microbes and their interactions with the host (Integrative, 2014). Accordingly, the gut microbiome has been shown to play causative role in the most prominent diseases of modern times, including inflammatory bowel diseases (IBD) such as Crohn's and ulcerative colitis, colon cancer and metabolic diseases such as diabetes and obesity (Cho and Blaser, 2012). However, attempts to identify a common pattern of microbial dysbiosis linked with these diseases have failed. Recently, multiple studies have shown that bacterial communities in the gut are spatially organized and disrupted spatial organization of the gut microbiome is often a common underlying feature of disease pathogenesis. As a result, focus over the last few years has shifted towards understanding gut microbiome dysbiosis in spatial context as a feature of microbiome associated diseases from just cataloging the diversity of gut bacteria (Donaldson et al., 2016). This line of investigation has brought the role of microbial communities overlying the intestinal mucus in promoting disease into sharp focus. A study involving the largest cohort of pediatric Crohn's disease patients demonstrated that assessing the mucus-associated microbiome compared to fecal communities is more effective in early diagnosis of disease (Gevers et al., 2014). Isolation of colonic mucus from mice mono-colonized with specific commensals showed that bacterial species present in the mucus show differential proliferation and resource utilization compared with the same species in the intestinal lumen of mice (Li et al., 2015). In both mouse and human it was shown that mucus-associated communities were distinct and not represented by fecal communities (Zmora et al., 2018). Moreover, mucosal communities were refractory to colonization by probiotics unless perturbed by antibiotics (Suez et al., 2018). Although these

studies underscore the critical role of mucus residing communities in determining disease pathology and promoting colonization resistance, ecological features of mucus resident communities that confer these properties remain poorly defined.

To fill this gap in our understanding of the gut microbiome ecology, we developed a novel strategy that combines fluorescence in-situ hybridization (FISH) with the spatial dissection power of laser capture microdissection (LCM) and 16S microbiome sequencing. We found that the microbial community closest to the host overlying the dense mucus layer forms a unique biofilm-like structure that harbors significantly higher species richness, selectively excluding bacteria belonging to class Gammaproteobacteria and is resistant to antibiotic induced dysbiosis. We propose that this community represents a previously unrecognized ecological safe harbor that promotes gut microbial homeostasis.

Results

Bacteria overlying the colonic mucus form biofilm-like structure that resists perturbation caused by broad spectrum antibiotic but not narrow spectrum antibiotic.

Fluorescence *in-situ* hybridization (FISH) to 16s rRNA in combination with specialized tissue fixation methodologies that preserve mucus structure in an intact state enable the observation of microbe-microbe and host-microbe relationships *in-situ* (Johansson et al., 2008; Mark Welch et al., 2016; Vaishnava et al., 2011). To understand the landscape of bacterial communities residing within the gut, we analyzed in the transverse sections of mouse colon using universal 16s rRNA FISH probes (Figure 1A). Quantification showed that the dense community extends up to 29 μm into the lumen forming a biofilm-like structure (Figure 1B). The biofilm resided immediately adjacent to the sterile, dense mucus layer (Figure 1C), which was on average 17μm thick in mice from our colony at Brown University (Figure 1D). To see if the biofilm-like structure close to the host was specific to mice in our colony, we evaluated the spatial organization of mice from Jackson Laboratories. We found that even though mice from

Jackson had a thinner dense mucus layer (average 4.6μm) they still had a similar biofilm-like community structure adjacent to the dense mucus layer that extends up to 33 μm (Figure S1). A similar dense community has previously been described in the colon of gnotobiotic mice colonized with a defined 15-member community (Mark Welch et al., 2017) suggesting that this is a conserved feature of gut microbial community organization.

In order to assess the contribution of community composition in the maintenance of the biofilm-like structure, we subjected it to perturbation by a broad (Ciprofloxacin) and narrow (Vancomycin) spectrum antibiotic (Figure S2A). Comparison of fecal communities of mice treated with Vancomycin or Ciprofloxacin to that of untreated communities confirmed that both antibiotics significantly decreased the diversity of the microbiome, a characteristic of antibiotic treatment (Figure S2B). The mice treated with Vancomycin experienced a larger disruption in fecal community composition compared to those treated with Ciprofloxacin (Figure S2C). Vancomycin treatment as expected resulted in a significant depletion of Clostridia and an expansion of Gammaproteobacteria (Table S1 and S2). To determine if differences in community composition between Ciprofloxacin and Vancomycin treatments correlated with differences in community structure, we employed FISH to visualize the gut microbiome *in-situ*. Ciprofloxacin treated communities maintained the biofilm-like structure similar to that seen in untreated mice, whereas this community structure was completely lost in mice treated with Vancomycin (Figures 1E, 1F and 1G). The Ciprofloxacin-treated mice were devoid of Proteobacteria whereas the remaining community in Vancomycin-treated mice harbored members of Proteobacteria (Figures 1E, 1F, 1H). Additionally, Clostridia were preserved within the biofilm community upon Ciprofloxacin treatment, but lost after Vancomycin treatment (Figures 1E ,1F and 1I). Obliteration of the biofilm-like structure was inversely correlated with the presence of Clostridia within the dense community. These data suggest that vancomycin-sensitive microbes such as Clostridia are important for maintaining community structure.

Mucus associated biofilm community is compositionally distinct from adjoining non-biofilm community.

To assess the microbial composition of the bacterial community in the mucus biofilm we adapted laser-capture microdissection (LCM) technique to isolate defined regions of the colonic mucus layer followed by 16S rRNA sequencing. The LCM isolation strategy was designed so as to capture the first 100µm from the epithelial lining (corresponding to the observed thickness of the biofilm) (inner) independently of the adjoining 50µm section of non-biofilm community (outer) (Figure 2A-B). Using this strategy, we collected an area of 1,000,000 μm^2 of the inner community and corresponding 500,000μm^2 of the outer community for each mouse colon. qPCR quantification of the community samples confirmed that the inner biofilm community had higher bacterial load compared to the outer non-biofilm community (Figure 2C). We applied similar dissection strategy to colonic tissue sections from germ-free(GF) mice to ensure that the LCM procedure did not introduce any bacterial DNA contamination (Figure S3). We isolated the inner biofilm and outer non-biofilm communities from mice from two different cages and compared microbiome dissimilarities based on cage and location (inner vs outer). We used the distance metric UniFrac that uses phylogenetic relationships to evaluate differences in overall composition between communities (Lozupone and Knight, 2005). Using weighted UniFrac distances that calculates dissimilarities in abundance of microbes (quantitative), we only saw a difference in community composition between the two cages but no difference was noted between the two locations (Figure 2D Left). The unweighted analysis that calculates dissimilarity based on presence or absence of a microbe (qualitative) showed that location was the second most contributing variable that significantly separated the biofilm community from the adjacent non-biofilm community (Axis 2) (Figure 2D Right). Evaluating composition without abundance indicates differences in communities is based on which taxa are able to live in them (Lozupone et al., 2007). Differential abundance analysis at class level revealed that the biofilm community just like the non-biofilm community comprised mainly of bacteria belonging to class Bacteroidia

and Clostridia. However, the non-biofilm community harbored significantly more Gammaproteobacteria compared to the biofilm community (Figure 2E-F). These results suggest that Gammaproteobacteria are selectively restricted from colonizing the mucus layer closest to the host epithelium.

Biofilm community closest to the host has significantly higher species richness due to presence of low abundance unique amplicon sequence variants (ASVs).

Diversity is one of the most important ecological attributes which determines stability of a community (Smith, 2007). The number of species represented in an ecosystem (its richness) and the way in which individuals are distributed amongst the species (its evenness) are often combined into a single index to quantify diversity. Plotting the number of unique amplicon sequence variants (ASVs) found at increasing subsampling depths with an alpha rarefaction curve showed that the biofilm community consistently had more unique observed ASVs (Figure 3A). Using the Chao1 index that estimates true community richness, we saw the inner community that corresponds with the biofilm has significantly higher species richness (Figure 3B). Species evenness in a community captures another aspect of diversity by determining diversity as a standardized index of relative species abundance. We evaluated the evenness of the two communities by applying Pielou's evenness index (Pielou, 1969) and found the biofilm community is significantly less even than the non-biofilm community (Figure 3D). Accordingly, Shannon-Weaver, a commonly used diversity index that takes into account both richness and evenness of communities, showed no difference between the two communities. (Figure 3C).

Given the high alpha diversity in the inner community, we hypothesized that the inner community might harbor microbial species that are not found in the outer community. To test this, we determined the number of ASVs that were unique or shared between the inner biofilm and outer non-biofilm community within each mouse. We found in each animal significantly more ASVs were unique to the biofilm (average 70% unique, 30% shared) (Figure 3E) whereas

the adjoining non-biofilm region comprised of more shared ASVs (30% unique and 70% shared). Bacteroidia and Clostridia made up the majority of bacteria that are unique or shared in both communities (Figure 3F). Additionally, at family level unique microbes made up a very small percent (<0.2%) of the total abundance within the biofilm community (Figure 3G). Conversely, microbes shared between the two locations were highly abundant within the biofilm (Figure S4). We believe that although unique mucus-associated bacteria are seeded from the luminal microbes, many microbial species in the lumen community might be too scarce to be captured by sequencing. As a result we detect these low abundant microbial species only when their relative abundance increases during biofilm formation. Thus our results demonstrate that mucus associated biofilms represent a novel species bank of hidden microbial diversity and functional potential in the gut.

Mucus residing biofilm community maintains higher species richness and is less prone to dysbiosis than luminal community following antibiotics

Uneven distribution or spatial heterogeneity of species within an ecosystem increase its stability during large scale perturbations (Wang and Loreau, 2014). We wanted to assess whether the spatial heterogeneity we observe within the gut mucosal community contributes to its stability. Mice from Jackson laboratories were subjected to a clinically relevant vancomycin treatment for 10 days (Sekirov et al., 2008)(Figure 4A). Taking into account the thinner mucus layer in Jackson mice, (Figure S1), we isolated the 50µm section closest to the intestinal epithelium. Luminal community was isolated by excising a 300µm diameter circle from the center of the cross section. Antibiotic treatment significantly altered the biofilm as well luminal communities (Figure 4B-C). Before antibiotic treatment communities in both locations had similar richness, however following antibiotic treatment the mucus biofilm community lost significantly less richness than luminal communities (Figure 4D). The greater impact of antibiotic treatment on species richness in the luminal community suggests the biofilm community is less

susceptible to antibiotic perturbation. Additionally, after antibiotic treatment, we saw an increase in the relative abundance of Proteobacteria and a decrease in the relative abundance of Firmicutes in the luminal community compared to the biofilm community (Figure 4E). Specifically, we saw that post antibiotic treatment, the differential abundance of Clostridia was significantly more in the biofilm than the lumen community (Figure 4F). In contrast, a larger bloom β-Proteobacteria was observed in the lumen compared to the biofilm (Figure 4G). Quantification with qPCR and Clostridia specific 16s rRNA FISH further confirmed that after antibiotic treatment significantly more Clostridia are preserved within the biofilm compared to lumen (Figure 4H-I).

Discussion

Biofilms constitute the dominant mode of microbial life in most ecosystems (Costerton et al., 1995; Hall-Stoodley et al., 2004) yet they remain poorly described in the gut that harbor dense consortium of commensal bacteria. To characterize complex gut biofilms, we used a classical histological procedure to preserve mucus integrity, specific techniques for microbiota detection (i.e., FISH) and UV-laser assisted dissection of biofilm communities in micron scale for 16s rRNA microbiome analysis. Our method using entire cross sections of mouse colon fixed in Carnoy's fixative to preserve mucus architecture allowed us to survey the structure and spatial composition of the gut microbiome as it exists *in-situ*. We saw that intestinal bacteria form a continuous biofilm, lining the mucus surface that coats the colonic mucosa. Biofilm structure was stable when treated with Ciprofloxacin, a broad-spectrum antibiotic, but collapsed completely when treated with Vancomycin that targets commensals belonging to class Clostridia. Collapse of biofilm structure coincided with bloom of Proteobacteria near the mucus. Our observation that mucus associated biofilm in the murine colon is a normal feature is in contrast to studies that associate intestinal biofilms with pathogenic phenotypes such as IBD and colon cancer (Dejea et al., 2018; Swidsinski et al., 2005). However in these studies it was

noted that the biofilms associated with diseased pathology had higher concentration of pathobionts such as *Bacteroides fragilis*, *E.coli* and *Fusobacterium nucleatum* compared to controls. Moreover, biofilms from patients with Crohn's disease or with ulcerative colitis were shown to be disrupted, allowing pathobionts to spread and invade intestinal epithelia and cause inflammation (Motta et al., 2018). Thus, indicating that it is not the biofilm phenotype per se that drives the disease phenotype but structural and functional disruption of intestinal biofilms that drives disease pathogenesis in the gut. In fact, mucus associated biofilms provide an efficient strategy for commensals to resist environmental perturbations, the host immune system, and luminal flow in the GI tract and thus promote stability of the gut microbiota (Dunne, 2002). Additionally, close proximity of mucus associated biofilms benefit the host by modulating immunity and acting as deterrent to colonization and invasion by enteropathogens (Round and Mazmanian, 2009).

Using antibiotics with different targets we found that the "narrow-spectrum" antibiotic induced the largest changes in biofilm structure and the loss of biofilm structure was correlated with ablation of Clostridia and the expansion of Proteobacteria. These results suggest that "narrow-spectrum" and "broad-spectrum" require new definitions that go beyond understanding how antibiotics specifically target certain organisms, and incorporate how they affect community architecture. A number of healthy people naturally carry *Clostridium difficile* in their large intestine and don't have ill effects from the infection (Taylor et al., 1981). *C.difficile* infection in humans are associated with recent antibiotic use (De La Cochetiere et al., 2008). Once infected, *C.difficile* is known to form biofilms in the gut that resist antibiotic treatment (Ethapa et al., 2013). It would be important to understand whether the adverse effect of an antibiotic regimen on the commensal biofilm is directly correlated with susceptibility to *C.difficile* infection. Also equally important to determine would be whether fecal microbiota transfer (FMT) that corrects *C.difficile* infection restores homeostatic commensal biofilm.

16s rRNA microbiome analysis of the bacterial community micro-dissected from the biofilm revealed that Gammaproteobacteria, a bacterial class associated with antibiotic induced dysbiosis, are in much lower abundance in the biofilm compared to adjoining areas. In a healthy gut, members of phylum Proteobacteria are normally maintained at very low levels but expand significantly in dysbiosis (Le Bastard et al., 2018; Rivera-Chavez et al., 2017). Increased abundance of class Gammaproteobacteria is seen in metabolic disorders (Larsen et al., 2010; Qin et al., 2012), obesity (Fei and Zhao, 2013; Sen et al., 2017), and inflammatory bowel disease (Gevers et al., 2014), all pathologies characterized by intestinal inflammation (Sen et al., 2017). Our results suggest that biofilm structure rich in anaerobic commensals such as Clostridia suppress Proteobacteria bloom. Depletion of Clostridia within the biofilm is coincident with Proteobacteria bloom. We also found that antibiotic induced depletion of species richness and associated dysbiosis was significantly lower in biofilm compared to the lumen communities. Several studies show that biofilm-grown cells have properties that are distinct from planktonic cells, one of which is an increased resistance to antimicrobial agents (Donlan, 2002) . Work on *in-vitro* biofilms show that slow growth and/or induction of an rpoS-mediated stress response could contribute to antimicrobial resistance (Prigent-Combaret et al., 1999). Moreover, the physical and/or chemical structure of mucus where the biofilms are embedded could also confer resistance by exclusion of antibiotics from the bacterial community. Finally, bacteria growing as biofilm might develop a specific antibiotic-resistant phenotype (Olsen, 2015). It is likely that there are multiple resistance mechanisms at work that confer this property to mucus biofilms and future work looking at meta-transcriptional response of mucus associated biofilms in health and disease would be crucial in further delineating these properties.

Mechanisms regulating the biofilm formation of commensal bacteria are yet to be fully elucidated. Whether these mechanisms are bacteria or/and host intrinsic remains to be seen. Bacterial intrinsic mechanisms such as expression of Serine-Rich Repeat Proteins (SRRP's) that bind to host epithelial proteins in pH-dependent manner can be foreseen in helping biofilm

formation in different niches of the gut (Frese et al., 2013; Sequeira et al., 2018). Another bacterial intrinsic mechanism that could be crucial for biofilm formation is a mode of biochemical communication between different bacteria species called quorum sensing. The role of quorum sensing has been well established in forming biofilms in several bacterial species, including *E. coli*, *P. aeruginosa*, and *Salmonella sp*. (Valentini and Filloux, 2016). Quorum sensing between different species of gut commensals was recently shown to influence the abundance of the major phyla of the gut microbiota (Thompson et al., 2015). On the host side, several innate and adaptive immune effectors that are continuously secreted into the gut lumen could play a role in entrenching the biofilm in the intestinal mucus. Whether the huge quantity of IgA that is secreted into the gut lumen contributes to complex biofilm formation requires further research. Recently it was shown that *in vivo* coating with IgA promotes aggregation of commensal bacteria *B.fragilis* within the mucus (Donaldson et al., 2018). A different study linked IgA binding to bacteria within the mucus layer of the colon to transcriptional changes that stabilize in microbial consortium (Nakajima et al., 2018). Gut epithelium also secretes a slew of antimicrobial proteins that are important for regulating spatial organization of bacteria that could play a critical role in biofilm formation. For example, RegIIIγ, a c-type lectin that specifically targets Gram positive bacteria regulates host-microbe spatial segregation in the small intestine could promote biofilm structure by maintaining immune tolerance of microbial communities close to the epithelium (Vaishnava et al., 2011). A small lectin-like protein ZG16 (zymogen granulae protein 16) secreted by the host was recently shown to aggregate bacteria in the colonic mucus layer to maintain bacteria at a safe distance from the epithelial cell surface (Bergstrom et al., 2016). Finally, epithelium secreted effector Ly6/PLAUR domain containing 8 (Lypd8) protein binds flagellated microbiota and keeps them away from epithelium (Okumura et al., 2016). These and other discoveries on the mechanisms orchestrating the gut microbiota spatial organization should be evaluated for their role in promoting homeostatic biofilms in the gut. Determining mechanisms that promote or

disrupt homeostatic biofilm structure in gut should help towards identifying novel therapeutic targets in a broad variety of disorders mediated by microbiota biofilm dysbiosis.

STAR Methods

Contact for Reagent and Resource Sharing

Further information and requests for resources and reagents should be directed to and will be fulfilled by the Lead Contact, Dr. Shipra Vaishnava (shipra_vaishnava@brown.edu).

Experimental Model and Subject Details

Mice

All mice used were wild-type with a C57BL/6 background. Mice used for homeostatic characterization were bred in the SPF barrier facility at Brown University and sacrificed at 8 weeks of age. 6 mice were male, all littermates and kept in the same cage. The other 5 were female from two different litters and kept in the same cage post-weaning (cage-mates). Mice used for characterization of spatial organization in Jackson mice were ordered from Jackson Laboratories, consisting of 3 males and 3 females and sacrificed at 6 weeks of age. Mice used for comparing mucosal and luminal communities after antibiotic treatment were ordered from Jackson Laboratories, consisting of 15 6-week old female cage-mates. Mice used for comparing Ciprofloxacin and Vancomycin antibiotic treatment were ordered from Taconic Biosciences, consisting of 12 7-week old female cage-mates. Experiments were performed according to protocols approved by the Institutional Animal Care and Use Committees of Brown University.

Antibiotics Experiments

Experiment comparing Vancomycin and Ciprofloxacin antibiotic treatment was done by exchanging drinking water with either 500mg/L Vancomycin or 500mg/L Ciprofloxacin (pH 11). Mice were sacrificed after 3 days of treatment. Experiment comparing mucosal and luminal

communities after antibiotic treatment was done by exchanging drinking water with 100mg/L Vancomycin. Mice were sacrificed after 10 days of treatment.

Method Details

Sample Preparation

The distal colon was carefully removed to avoid disrupting architecture of encased contents and placed in 3mL Methacarn for 24 hours. Tissues were washed 3x over 3 days with 70% EtOH at 4°C. Tissues were processed at the Brown University Molecular Pathology Core with the Leica ASP300S by first dehydrating (70% EtOH 1 hr, 2 washes 95% EtOH 45 min, 1 hr, 3 washes 100% EtOH 45 min, 1 hr, 1 hr) then infiltrated with xylenes (3 washes, 45 min, 45 min, 1 hr) followed by paraffin wax at 60°C (1 hr, 1 hr, 1hr 15 min). Samples were embedded in paraffin to produce cross sections by holding tissues vertically in a base of hot wax while chilling. Once wax base secured the tissue vertically, the cassette was filled the rest of the way and chilled until hard.

Fluorescence in-situ hybridization and MFI Quantification

7-µm thick slides were deparaffinized through a solution series for 10 minutes each (xylenes, xylenes, 100% EtOH, 95% EtOH, 70% EtOH, H_2O). Slides were placed in a pre-warmed (56°C) humidifying chamber and incubated 10 minutes with pre-warmed hybridization buffer (0.9M NaCl, 20mM Tris pH 7.4, 0.1% SDS). Hybridization buffer was removed and pre-warmed probe solutions were applied to regions of tissue isolated with hydrophobic slider marker. Probe solutions were prepared using 2µL EUB338I (1µg/µL), 2µL EUB338II (1µg/µL), 2 µL EUB338III (1µg/µL), and 94µL hybridization buffer per slide for viewing all bacteria (green) (Daims et al., 1999); 2µL EUB338I (1µg/µL), 2µL EUB338II (1µg/µL), 2 µL EUB338III (1µg/µL), 2µL GAM42a (1µg/µL) , 2µL BET42a (1µg/µL), 35µL formamide, and 55µL hybridization buffer per slide for viewing all bacteria (green) and Proteobacteria (red) (Manz et al., 1992); 2µL EUB338-I

(1µg/µL), 2µL EUB338-II (1µg/µL), 2 µL EUB338III (1µg/µL), 2µL Clep866 (1µg/µL), 2µL Erec482 (1µg/µL), 30µL formamide, and 60µL hybridization buffer per slide for viewing all bacteria (green) and Clostridia (red) (Franks et al., 1998; Lay et al., 2005). Incubated slides at 56°C with probe solutions in humidifying chamber for 4 hours. Washed slides twice for 10 minutes in wash buffer (0.9M NaCl, 20mM Tris pH 7.4). Incubated slides with DAPI (1µg/mL) 10 minutes, followed by a final wash in wash buffer for 10 minutes. Dried slides 10 minutes at 56°C before applying coverslip with Fluro-Gel. Mean Fluorescence Intensity (MFI) measurements were taken using a Zeiss Inverted Microscope (Axio Observer Z1) using the profile function within the AxioVision Rel. 4.8 software to take the average MFI of the default 10-µm wide area, starting 10µm prior to the presence of bacteria and 40µm into the luminal space. 20 measurements were taken per mouse, taking 4 measurements from 5 different cross sections to obtain an average. Confocal images were taken on an Olympus FV3000 confocal microscope.

Mucus Thickness

7-µm thick slides were deparaffinized through a solution series for 5 minutes each (xylenes, xylenes, 100% EtOH, 95% EtOH, 75% EtOH, H_2O). Alcian Blue/Pas staining was done using the protocol outlined in “Histotechnology: A Self-Instructional Text, 3rd edition. Pages 115-116”. Slides were stained with Alcian Blue for 30 minutes, washed with running tap water for 2 minutes followed by a rinse with deionized (DI) water. Slides were stained with 0.5% Periodic acid for 5 minutes, washed with DI, then stained with Schiff’s Reagent for 30 minutes followed by a rinse with running tap water for 3 minutes. Nuclei were stained with Hematoxylin for 2 minutes, washed with running water for 30 seconds, followed by 10 dips in Clarifier, another 30 second wash, 10 dips in Bluing Reagent, and a final 30 second wash. Slides went through a solution series for 5 minutes each (95% EtOH, 100% EtOH, Xylenes, Xylenes). Coverslips were applied with Cytoseal and slides were allowed to dry overnight in the fume hood. The dense mucus layer of 40 locations evenly distributed from available cross sections on the slide (4-8

cross sections) were measured for each mouse at 60X magnification to obtain the average mucus thickness for each mouse, then combined to obtain the overall average and standard deviation.

Laser Capture Microdissection (LCM) and DNA extraction

Tissues were sectioned at 12µm and placed on Arcturus PEN Membrane Frame Slides and kept at 56°C overnight. Slides were deparaffinized through a solution series for 3 minutes each (xylenes, xylenes, 1:1; xylenes: EtOH, 100% EtOH, 100% EtOH, 95% EtOH, 70% EtOH, 50% EtOH, H_2O). Slides were stained with Alcian Blue (1 min), rinsed, and Nuclear Fast Red (15 sec), then allowed to dry 2 hours. Regions of intestinal content were isolated and removed with the Applied Biosystems Arcturus Laser Capture Microdissection (LCM) system. Like-regions were pooled on LCM Caps from multiple cross sections of the same mouse until approximately 2,000,000 μm^2 for 100-µm regions and 1,000,000 μm^2 for 50-µm regions were collected. Isolated material was placed on Eppendorf tubes containing solutions from the QIAamp DNA Micro Kit with the addition of 3µL 10mg/mL lysozyme and incubated 16 hours at 56°C. DNA was isolated following instructions of DNA Micro Kit and eluted with 30µL DNase-treated water.

Copy number of 16S rRNA per sample quantification

PCR amplified 16S rRNA gene from mouse fecal sample using Taq polymerase as described in the TOPO TA Cloning Kit User Guide with 16S rRNA Universal primers recognizing 340F and 515R (Amann et al., 1990). Cloned PCR product into a pCR 2.1-TOPO vector using the TOPO TA Cloning Kit and transformed recombinant vector into One Shot TOP10 Chemically Competent *E.coli* as described in the TOPO TA Cloning Kit User Guide. Isolated plasmid DNA with the Invitrogen PureLink Quick Plasmid Miniprep Kit. Checked 16S rRNA gene properly inserted into vector with PCR using M13 reverse primer provided in TOPO TA Cloning Kit and 16S rRNA Universal primer 515R and with EcoR1 restriction digest following protocol provided

with restriction enzyme. Generated a standard curve using quantitative PCR and primers 340F and 515R with plasmid DNA of known concentrations, relating DNA concentration to copy number using the equation provided in Park and Crowley, 2005. Found the best fit line between CT value vs. copy number in order to relate the CT value of the unknown sample values to copy number.

16S Amplicon Sequencing

Isolated DNA was amplified (30 cycles) using the Phusion High-Fidelity DNA Polymerase. Primers were designed to contain adapter overhangs complimentary for Nextera XT tagmentation with the locus-specific sequencing flanking the V4/V5 region of the 16S rRNA gene (518F and 926R). PCR products were cleaned with Ampure XP and visualized by agarose gel electrophoresis. A second round of PCR (up to 50ng of template DNA, 5-10 cycles) was performed to attach full indices and adapters using the Nextera XT Index Kit and Phusion HF Master Mix. PCR products from the second PCR were cleaned with Ampure XP and analyzed by agarose gel electrophoresis and the Agilent BioAnalyzer DNA 1000 chip. Quantification and normalization was performed on all samples prior to pooling using Qubit fluorometer and the final pooled library was quantified using qPCR in a Roche LightCycler 480 with the KAPA Biosystems Illumina Kit. Samples were sequenced (2x250 bp paired-end) on an Illumina MiSeq at the Rhode Island Genomics and Sequencing Center (Kingston, RI).

Bioinformatics

Quality control of raw sequences was performed using dada2 package v1.6.0 (Callahan et al., 2016) in R v3.4.3. Forward and reverse reads were truncated to be 240bp and 190bp, respectively. The first 20bp were also removed to remove where primers bound constant regions, and standard filtering parameters were applied (Anders and Huber, 2010). Sequences were denoised by estimating error rates from pooled sequencing reads from all samples

provided. Reads were then merged and chimeras identified and removed. Taxonomy was assigned using the RDP training set(Wang et al., 2007). The rooted phylogenetic tree was created using ape package v5.1 (Paradis et al., 2004). Data were imported and analyzed using phyloseq v1.22.3 (McMurdie and Holmes, 2013). Principal Coordinates of Analysis (PCoA) plots were made by calculating distances between communities using UniFrac (Lozupone and Knight, 2005) and transforming sample counts into percentages to normalize for unequal sampling depth. Alpha-diversity tests (Observed ASVs, Shannon, Pielou's Evenness) were done on samples rarefied to the sample with the lowest sequencing depth. Raw values were exported to Prism to make final figures.

Quantitative PCR

Samples were prepared using Maxima SYBR Green/ROX qPCR Master Mix following the protocol outlined in the Maxima SYBR Green/ROX qPCR Master Mix User Guide. Relative abundance of Clostridia was determined using mix of CI-F1/CI-R2, CXI-F1/CXI-R2, and CIV-F1/CIV-R2 primer sets (Song et al., 2004). Values were normalized to 16S rRNA Universal (340F and 515R).

Quantification and Statistical Analysis

Differences between groups of communities was calculated using a permutational multivariate analysis of variance (PERMANOVA) based on UniFrac distance (Lozupone and Knight, 2005). Differential abundance was calculated using DESeq2 (Love et al., 2014), determining the adjusted p-value for multiple comparisons threshold as ≤ 0.05. All other significance tests were done using a parametric t-test, using a paired t-test when applicable.

Data and Software Availability

Raw reads have been deposited in the NCBI Sequence Read Archive (SRA) database under the BioProject ID number PRJNA545452. Data and code is available on the Vaishnava lab GitHub page (https://github.com/vaishnavalab/Biogeography).

Key Resource Table

REAGENT or RESOURCE	SOURCE	IDENTIFIER
Antibodies		
DAPI	Life tech	Cat#: D1306
Betaproteobacteria probe: BET42a Alexa 546 Red GCCTTCCCACTTCGTTT	Manz et al. 1992	NA
Clostridium leptum subgroup: Clep866 Alexa 546 Red GGTGGATWACTTATTGTG	Lay et al., 2005	NA
Clostridium coccoides-Eubacterium rectale group: Erec482 Alexa 546 Red GCTTCTTAGTCARGTACCG	Franks et al., 1998	NA
Universal bacterial probe (16S rRNA): EUB338-I Alexa 488 Green GCTGCCTCCCGTAGGAGT	Daims et al. 1999	NA
Universal bacterial probe (16S rRNA): EUB338-II Alexa 488 Green GCAGCCACCCGTAGGTGT	Daims et al. 1999	NA
Universal bacterial probe (16S rRNA): EUB338-III Alexa 488 Green GCTGCCACCCGTAGGTGT	Daims et al. 1999	NA
Gammaproteobacteria probe: GAM42a Alexa 546 Red GCCTTCCCACATCGTTT	Manz et al. 1992	NA
Bacterial and Virus Strains		
Salmonella Typhimurium (*S. enterica* serovar *Typhimurium*)	UT. South Western Dr. Vanessa Sperandio	Strain: SL1344
Chemicals, Peptides, and Recombinant Proteins		
Agencourt AMPure XP	Beckman Coulter Life Sciences	Cat#: A63882
Alcian Blue Solution, pH 2.5	American MasterTech	Cat#: 70800-201
Ampicillin, Sodium Salt	Fisher Scientific	Cat#: BP1760-25
Bluing Reagent	ThermoFisher Scientific	Cat#: 7301
Ciprofloxacin, 98%, Acros Organics	ThermoFisher Scientific	Cat#: AC449620050 Lot#: A0355311
Clarifier 2	ThermoFisher Scientific	Cat#: 7402

EcoR1	Promega	Cat#: R6011
Formamide, ≥99.5% (GC)	Sigma Aldrich	Cat#:F9037-100ML
Hematoxylin 2	Fisher HealthCare	Cat#: 22-220-102
HL-dsDNase	ArcticZymes	Cat#: 70800-201
Invitrogen Taq DNA Polymerase	Fisher Scientific	Cat#: 10-342-020
Lysozyme	ThermoFisher Scientific	Cat#: 89833
Methacarn	Fisher Scientific	Cat#: NC0547175
Nuclear Fast Red	Sigma Aldrich	Cat#: N3020
Periodic Acid, 1% Aqueous	Electron Microscopy Sciences	Cat#: 26853-02
Phusion High-Fidelity DNA Polymerase	ThermoFisher Scientific	Cat#: F530L
Schiff's Reagent	Electron Microscopy Sciences	Cat#: 26774-01
Vancomycin	ThermoFisher Scientific	Cat#: AAJ6279006
Critical Commercial Assays		
Agilent DNA 1000 Kit	Agilent	Cat#: 5067-1504
KAPA Library Quantification Kit	KAPA Biosystems	Cat#: KK4854
Maxima SYBR Green/ROX qPCR Master Mix	ThermoFisher Scientific	Cat#: K0221
MiSeq Reagent Kits v3 (600-cycles)	Illumina	Cat#: MS-102-3003
Nextra XT Index Kit	Illumina	Cat#: FC-131-1001
PureLink Quick Plasmid Miniprep Kit	ThermoFisher Scientific	Cat#: K210010
QIAamp DNA Micro Kit	Qiagen	Cat#: 56304
Qubit dsDNA HS Assay Kit	ThermoFisher Scientific	Cat#: Q32854
Quick-DNA Fungal/Bacterial Microprep Kit	Zymo Research	Cat#: D6007
TOPO TA Cloning Kit for Subcloning with One Shot TOP10 chemically competent *E.coli* cells	ThermoFisher Scientific	Cat#: K450001
Deposited Data		
Data and code	This paper	https://github.com/vaishnavalab/Biogeography
Raw sequencing data	This paper	NCBI Sequence Read Archive (SRA) BioProject: PRJNA545452
Experimental Models: Organisms/Strains		
C57Bl/6 Mice	Jackson Laboratories	Stock # 000664
C57Bl/6 Mice	Taconic BioSciences	Strain C57BL/6NTac
Oligonucleotides		
CI-F1 Clostridia cluster I: TACCHRAGGAGGAAGCCAC	Song et al., 2004	NA

CI-R2 Clostridia cluster I: GTTCTTCCTAATCTCTACGCAT	Song et al., 2004	NA
CXI-FI Clostridia cluster XI: ACGCTACTTGAGGAGGA	Song et al., 2004	NA
CXI-R2 Clostridia cluster XI: GAGCCGTAGCCTTTCACT	Song et al., 2004	NA
CIV-F1 Clostridia cluster XIVab: GAWGAAGTATYTCGGTATGT	Song et al., 2004	NA
CIV-R2 Clostridia cluster XIVab: CTACGCWCCCTTTACAC	Song et al., 2004	NA
340F 16S rRNA Universal: ACTCCTACGGGAGGCAGCAGT	Amann et al., 1990	NA
514R 16S rRNA Universal: ATTACCGCGGCTGCTGGC	Amann et al., 1990	NA
518F with Nextra recognizable regions: TCGTCGGCAGCGTCAGATGTGTATAAGAG ACAGCCAGCAGCYGCGGTAAN	https://vamps.mbl.edu/ resources/primers.php	NA
926R with Nextra recognizable regions: GTCTCGTGGGCTCGGAGATGTGTATAAGA GACAGCCGTCAATTCNTTTRAGT	https://vamps.mbl.edu/ resources/primers.php	NA
Software and Algorithms		
Package ‘Ape’	Bioconductor	https://cran.r-project.org/web/packages/ape/ape.pdf
AxioVision Rel. 4.8 Software	Fisher Scientific	Cat#: 11875113
DADA2	Callahan et al., 2016	https://benjjneb.github.io/dada2/index.html
DESeq2	Bioconductor	https://bioconductor.org/packages/release/bioc/html/DESeq2.html
GraphPad Prism 7	GraphPad Software Inc.	RRID: SCR_002798
Phyloseq	Phyloseq R Package	https://www.bioinformatics.babraham.ac.uk / projects/fastqc/; RRID: SCR_014583
R 3.4.3	The R Foundation	https://www.r-project.org/
Ribosomal Database Project (RDP) Training Set 16	Cole et al., 2014	https://rdp.cme.msu.edu/
Other		
Arcturus PEN Membrane Frame Slides	ThermoFisher Scientific	Cat#: LCM0521
CapSure Macro LCM Caps	ThermoFisher Scientific	Cat#: LCM0211
Cytoseal XYL	ThermoFisher Scientific	Cat#: 22-050-262

Fluoro-Gel (with Tris Buffer)	Electron Microscopy Sciences	Cat#: 17985-10
Parablocks ASP 300 Paraffin Wax	Leica Biosystems	Cat#: 39V2001

Acknowledgments: We thank Dr. Namrata Iyer for helpful discussions and Dr. Jim Mossman for statistical advice. We also thank Janet Atoyan for preparing libraries and sequencing, Geoffrey Williams for assistance with confocal microscopy, and members of the Brown University Histology Core, Paula Weston, Mindie Golde, and David Silverberg for sample preparation. This work was supported by NIH (P20GM10903 and 1R01DK113265 to S.V.) and DoD (W81XWH-18-1-0281 to S.V). S.V., K.D, and K. C. E designed experiments and performed analysis. S.V and K.D. wrote the manuscript.

References

Amann, R.I., Binder, B.J., Olson, R.J., Chisholm, S.W., Devereux, R., and Stahl, D.A. (1990). Combination of 16S rRNA-targeted oligonucleotide probes with flow cytometry for analyzing mixed microbial populations. Appl Environ Microbiol *56*, 1919-1925.

Anders, S., and Huber, W. (2010). Differential expression analysis for sequence count data. Genome Biol *11*, R106.

Bergstrom, J.H., Birchenough, G.M., Katona, G., Schroeder, B.O., Schutte, A., Ermund, A., Johansson, M.E., and Hansson, G.C. (2016). Gram-positive bacteria are held at a distance in the colon mucus by the lectin-like protein ZG16. Proc Natl Acad Sci U S A *113*, 13833-13838.

Callahan, B.J., McMurdie, P.J., Rosen, M.J., Han, A.W., Johnson, A.J., and Holmes, S.P. (2016). DADA2: High-resolution sample inference from Illumina amplicon data. Nat Methods *13*, 581-583.

Cho, I., and Blaser, M.J. (2012). The human microbiome: at the interface of health and disease. Nat Rev Genet *13*, 260-270.

Costerton, J.W., Lewandowski, Z., Caldwell, D.E., Korber, D.R., and Lappin-Scott, H.M. (1995). Microbial biofilms. Annu Rev Microbiol *49*, 711-745.

Daims, H., Brühl, A., Amann, R., Schleifer, K.-H., and Wagner, M. (1999). The Domain-specific Probe EUB338 is Insufficient for the Detection of all Bacteria: Development and Evaluation of a more Comprehensive Probe Set. Systematic and Applied Microbiology *22*, 434-444.

De La Cochetiere, M.F., Durand, T., Lalande, V., Petit, J.C., Potel, G., and Beaugerie, L. (2008). Effect of antibiotic therapy on human fecal microbiota and the relation to the development of Clostridium difficile. Microb Ecol *56*, 395-402.

Dejea, C.M., Fathi, P., Craig, J.M., Boleij, A., Taddese, R., Geis, A.L., Wu, X., DeStefano Shields, C.E., Hechenbleikner, E.M., Huso, D.L.*, et al.* (2018). Patients with familial adenomatous polyposis harbor colonic biofilms containing tumorigenic bacteria. Science *359*, 592-597.

Donaldson, G.P., Ladinsky, M.S., Yu, K.B., Sanders, J.G., Yoo, B.B., Chou, W.C., Conner, M.E., Earl, A.M., Knight, R., Bjorkman, P.J.*, et al.* (2018). Gut microbiota utilize immunoglobulin A for mucosal colonization. Science *360*, 795-800.

Donaldson, G.P., Lee, S.M., and Mazmanian, S.K. (2016). Gut biogeography of the bacterial microbiota. Nat Rev Microbiol *14*, 20-32.

Donlan, R.M. (2002). Biofilms: microbial life on surfaces. Emerg Infect Dis *8*, 881-890.

Dunne, W.M., Jr. (2002). Bacterial adhesion: seen any good biofilms lately? Clin Microbiol Rev *15*, 155-166.

Ethapa, T., Leuzzi, R., Ng, Y.K., Baban, S.T., Adamo, R., Kuehne, S.A., Scarselli, M., Minton, N.P., Serruto, D., and Unnikrishnan, M. (2013). Multiple factors modulate biofilm formation by the anaerobic pathogen Clostridium difficile. J Bacteriol *195*, 545-555.

Fei, N., and Zhao, L. (2013). An opportunistic pathogen isolated from the gut of an obese human causes obesity in germfree mice. Isme j *7*, 880-884.

Franks, A.H., Harmsen, H.J., Raangs, G.C., Jansen, G.J., Schut, F., and Welling, G.W. (1998). Variations of bacterial populations in human feces measured by fluorescent in situ hybridization with group-specific 16S rRNA-targeted oligonucleotide probes. Applied and environmental microbiology *64*, 3336-3345.

Frese, S.A., Mackenzie, D.A., Peterson, D.A., Schmaltz, R., Fangman, T., Zhou, Y., Zhang, C., Benson, A.K., Cody, L.A., Mulholland, F.*, et al.* (2013). Molecular characterization of host-specific biofilm formation in a vertebrate gut symbiont. PLoS Genet *9*, e1004057.

Gevers, D., Kugathasan, S., Denson, L.A., Vazquez-Baeza, Y., Van Treuren, W., Ren, B., Schwager, E., Knights, D., Song, S.J., Yassour, M.*, et al.* (2014). The treatment-naive microbiome in new-onset Crohn's disease. Cell Host Microbe *15*, 382-392.

Hall-Stoodley, L., Costerton, J.W., and Stoodley, P. (2004). Bacterial biofilms: from the natural environment to infectious diseases. Nat Rev Microbiol *2*, 95-108.

Integrative, H.M.P.R.N.C. (2014). The Integrative Human Microbiome Project: dynamic analysis of microbiome-host omics profiles during periods of human health and disease. Cell Host Microbe *16*, 276-289.
Johansson, M.E., Phillipson, M., Petersson, J., Velcich, A., Holm, L., and Hansson, G.C. (2008). The inner of the two Muc2 mucin-dependent mucus layers in colon is devoid of bacteria. Proc Natl Acad Sci U S A *105*, 15064-15069.
Larsen, N., Vogensen, F.K., van den Berg, F.W.J., Nielsen, D.S., Andreasen, A.S., Pedersen, B.K., Al-Soud, W.A., Sørensen, S.J., Hansen, L.H., and Jakobsen, M. (2010). Gut Microbiota in Human Adults with Type 2 Diabetes Differs from Non-Diabetic Adults. PLOS ONE *5*, e9085.
Lay, C., Sutren, M., Rochet, V., Saunier, K., Dore, J., and Rigottier-Gois, L. (2005). Design and validation of 16S rRNA probes to enumerate members of the Clostridium leptum subgroup in human faecal microbiota. Environ Microbiol *7*, 933-946.
Le Bastard, Q., Al-Ghalith, G.A., Gregoire, M., Chapelet, G., Javaudin, F., Dailly, E., Batard, E., Knights, D., and Montassier, E. (2018). Systematic review: human gut dysbiosis induced by non-antibiotic prescription medications. Aliment Pharmacol Ther *47*, 332-345.
Li, H., Limenitakis, J.P., Fuhrer, T., Geuking, M.B., Lawson, M.A., Wyss, M., Brugiroux, S., Keller, I., Macpherson, J.A., Rupp, S.*, et al.* (2015). The outer mucus layer hosts a distinct intestinal microbial niche. Nat Commun *6*, 8292.
Love, M.I., Huber, W., and Anders, S. (2014). Moderated estimation of fold change and dispersion for RNA-seq data with DESeq2. Genome Biol *15*.
Lozupone, C., and Knight, R. (2005). UniFrac: a new phylogenetic method for comparing microbial communities. Appl Environ Microbiol *71*, 8228-8235.
Lozupone, C.A., Hamady, M., Kelley, S.T., and Knight, R. (2007). Quantitative and qualitative beta diversity measures lead to different insights into factors that structure microbial communities. Appl Environ Microbiol *73*.
Manz, W., Amann, R., Ludwig, W., Wagner, M., and Schleifer, K.-H. (1992). Phylogenetic Oligodeoxynucleotide Probes for the Major Subclasses of Proteobacteria: Problems and Solutions. Systematic and Applied Microbiology *15*, 593-600.
Mark Welch, J.L., Hasegawa, Y., McNulty, N.P., Gordon, J.I., and Borisy, G.G. (2017). Spatial organization of a model 15-member human gut microbiota established in gnotobiotic mice. Proc Natl Acad Sci U S A *114*, E9105-e9114.
Mark Welch, J.L., Rossetti, B.J., Rieken, C.W., Dewhirst, F.E., and Borisy, G.G. (2016). Biogeography of a human oral microbiome at the micron scale. Proc Natl Acad Sci U S A *113*, E791-800.
McMurdie, P.J., and Holmes, S. (2013). phyloseq: an R package for reproducible interactive analysis and graphics of microbiome census data. PLoS One *8*, e61217.
Motta, J.P., Allain, T., Green-Harrison, L.E., Groves, R.A., Feener, T., Ramay, H., Beck, P.L., Lewis, I.A., Wallace, J.L., and Buret, A.G. (2018). Iron Sequestration in Microbiota Biofilms As A Novel Strategy for Treating Inflammatory Bowel Disease. Inflamm Bowel Dis *24*, 1493-1502.
Nakajima, A., Vogelzang, A., Maruya, M., Miyajima, M., Murata, M., Son, A., Kuwahara, T., Tsuruyama, T., Yamada, S., Matsuura, M.*, et al.* (2018). IgA regulates the composition and metabolic function of gut microbiota by promoting symbiosis between bacteria. J Exp Med *215*, 2019-2034.
Okumura, R., Kurakawa, T., Nakano, T., Kayama, H., Kinoshita, M., Motooka, D., Gotoh, K., Kimura, T., Kamiyama, N., Kusu, T.*, et al.* (2016). Lypd8 promotes the segregation of flagellated microbiota and colonic epithelia. Nature *532*, 117-121.
Olsen, I. (2015). Biofilm-specific antibiotic tolerance and resistance. Eur J Clin Microbiol Infect Dis *34*, 877-886.
Paradis, E., Claude, J., and Strimmer, K. (2004). APE: Analyses of Phylogenetics and Evolution in R language. Bioinformatics *20*, 289-290.

Prigent-Combaret, C., Vidal, O., Dorel, C., and Lejeune, P. (1999). Abiotic surface sensing and biofilm-dependent regulation of gene expression in Escherichia coli. J Bacteriol *181*, 5993-6002.
Qin, J., Li, Y., Cai, Z., Li, S., Zhu, J., Zhang, F., Liang, S., Zhang, W., Guan, Y., Shen, D.*, et al.* (2012). A metagenome-wide association study of gut microbiota in type 2 diabetes. Nature *490*, 55-60.
Rivera-Chavez, F., Lopez, C.A., and Baumler, A.J. (2017). Oxygen as a driver of gut dysbiosis. Free Radic Biol Med *105*, 93-101.
Round, J.L., and Mazmanian, S.K. (2009). The gut microbiota shapes intestinal immune responses during health and disease. Nat Rev Immunol *9*, 313-323.
Sekirov, I., Tam, N.M., Jogova, M., Robertson, M.L., Li, Y., Lupp, C., and Finlay, B.B. (2008). Antibiotic-induced perturbations of the intestinal microbiota alter host susceptibility to enteric infection. Infect Immun *76*, 4726-4736.
Sen, T., Cawthon, C.R., Ihde, B.T., Hajnal, A., DiLorenzo, P.M., de La Serre, C.B., and Czaja, K. (2017). Diet-driven microbiota dysbiosis is associated with vagal remodeling and obesity. Physiol Behav *173*, 305-317.
Sequeira, S., Kavanaugh, D., MacKenzie, D.A., Suligoj, T., Walpole, S., Leclaire, C., Gunning, A.P., Latousakis, D., Willats, W.G.T., Angulo, J.*, et al.* (2018). Structural basis for the role of serine-rich repeat proteins from Lactobacillus reuteri in gut microbe-host interactions. Proc Natl Acad Sci U S A *115*, E2706-E2715.
Smith, V.H. (2007). Microbial diversity–productivity relationships in aquatic ecosystems. FEMS Microbiology Ecology *62*, 181-186.
Song, Y., Liu, C., and Finegold, S.M. (2004). Real-time PCR quantitation of clostridia in feces of autistic children. Applied and environmental microbiology *70*, 6459-6465.
Suez, J., Zmora, N., Zilberman-Schapira, G., Mor, U., Dori-Bachash, M., Bashiardes, S., Zur, M., Regev-Lehavi, D., Ben-Zeev Brik, R., Federici, S.*, et al.* (2018). Post-Antibiotic Gut Mucosal Microbiome Reconstitution Is Impaired by Probiotics and Improved by Autologous FMT. Cell *174*, 1406-1423 e1416.
Swidsinski, A., Weber, J., Loening-Baucke, V., Hale, L.P., and Lochs, H. (2005). Spatial organization and composition of the mucosal flora in patients with inflammatory bowel disease. J Clin Microbiol *43*, 3380-3389.
Taylor, R.H., Borriello, S.P., and Taylor, A.J. (1981). Isolation of Clostridium difficile from the small bowel. Br Med J (Clin Res Ed) *283*, 412.
Thompson, J.A., Oliveira, R.A., Djukovic, A., Ubeda, C., and Xavier, K.B. (2015). Manipulation of the quorum sensing signal AI-2 affects the antibiotic-treated gut microbiota. Cell Rep *10*, 1861-1871.
Vaishnava, S., Yamamoto, M., Severson, K.M., Ruhn, K.A., Yu, X., Koren, O., Ley, R., Wakeland, E.K., and Hooper, L.V. (2011). The antibacterial lectin RegIIIgamma promotes the spatial segregation of microbiota and host in the intestine. Science *334*, 255-258.
Valentini, M., and Filloux, A. (2016). Biofilms and Cyclic di-GMP (c-di-GMP) Signaling: Lessons from Pseudomonas aeruginosa and Other Bacteria. J Biol Chem *291*, 12547-12555.
Wang, Q., Garrity, G.M., Tiedje, J.M., and Cole, J.R. (2007). Naive Bayesian classifier for rapid assignment of rRNA sequences into the new bacterial taxonomy. Applied and environmental microbiology *73*, 5261-5267.
Wang, S., and Loreau, M. (2014). Ecosystem stability in space: alpha, beta and gamma variability. Ecol Lett *17*, 891-901.
Zmora, N., Zilberman-Schapira, G., Suez, J., Mor, U., Dori-Bachash, M., Bashiardes, S., Kotler, E., Zur, M., Regev-Lehavi, D., Brik, R.B.*, et al.* (2018). Personalized Gut Mucosal Colonization Resistance to Empiric Probiotics Is Associated with Unique Host and Microbiome Features. Cell *174*, 1388-1405 e1321.

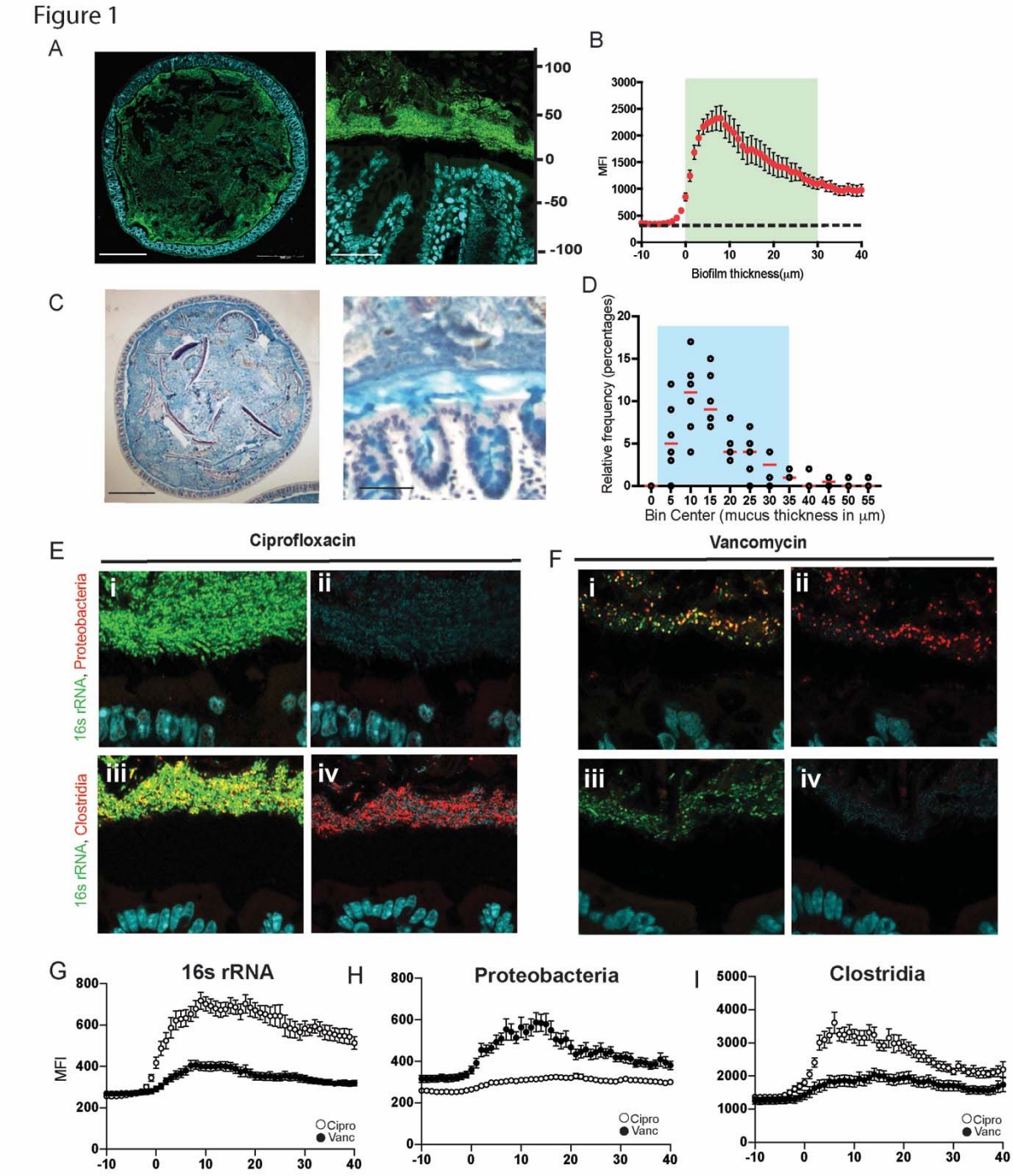

Figure 1. Bacterial community overlying the colonic mucus forms biofilm-like structure that is sensitive to vancomycin.

A. Colonic cross section stained with fluorescent probes identifying all bacteria (green) and host epithelium (blue) to show dense biofilm-like structure close to the host (Left: 10X: Right: 60X).

B. Mean fluorescence intensity (MFI) measurements from a representative mouse (average N=3) to show bacterial density of biofilm-like structure. Measurements start 10-μm before start of bacterial signal closest to epithelial lining.

C. Colonic cross section stained with Alcian Blue/Pas to show dense mucus layer (Left: 10X; Right: 60X).

D. Relative frequency of mucus thickness measurements (N=6, 40 measurements each)

E. FISH images of spatial structure after Ciprofloxacin treatment showing preservation of biofilm-like structure consisting of Clostridia and excluding Proteobacteria. *i*: merged image with host epithelium (blue), all bacteria (16S rRNA, green), and Proteobacteria (red). *ii*: merged image with host epithelium and Proteobacteria. *iii*: merged image with host epithelium, all bacteria, and Clostridia (red). *iv*: merged image with host epithelium and Clostridia.

F. FISH images of spatial structure after Vancomycin treatment showing decimation of biofilm-like structure as well as the absence of Clostridia and the prevalence of Proteobacteria. *i*: merged image with host epithelium (blue), all bacteria (16S rRNA, green), and Proteobacteria (red). *ii*: merged image with host epithelium and Proteobacteria. *iii*: merged image with host epithelium, all bacteria, and Clostridia (red). *iv*: merged image with host epithelium and Clostridia.

G-I. Mean fluorescence intensity (MFI) measurements for representative mice quantifying bacterial density of biofilm-like community by measuring fluorescence intensity of all bacteria (16s rRNA), Proteobacteria and Clostridia after Ciprofloxacin (open circles) and Vancomycin treatment (closed circles). Measurements started 10-μm before start of bacterial signal closest to epithelial lining (N=3).

Figure 2.

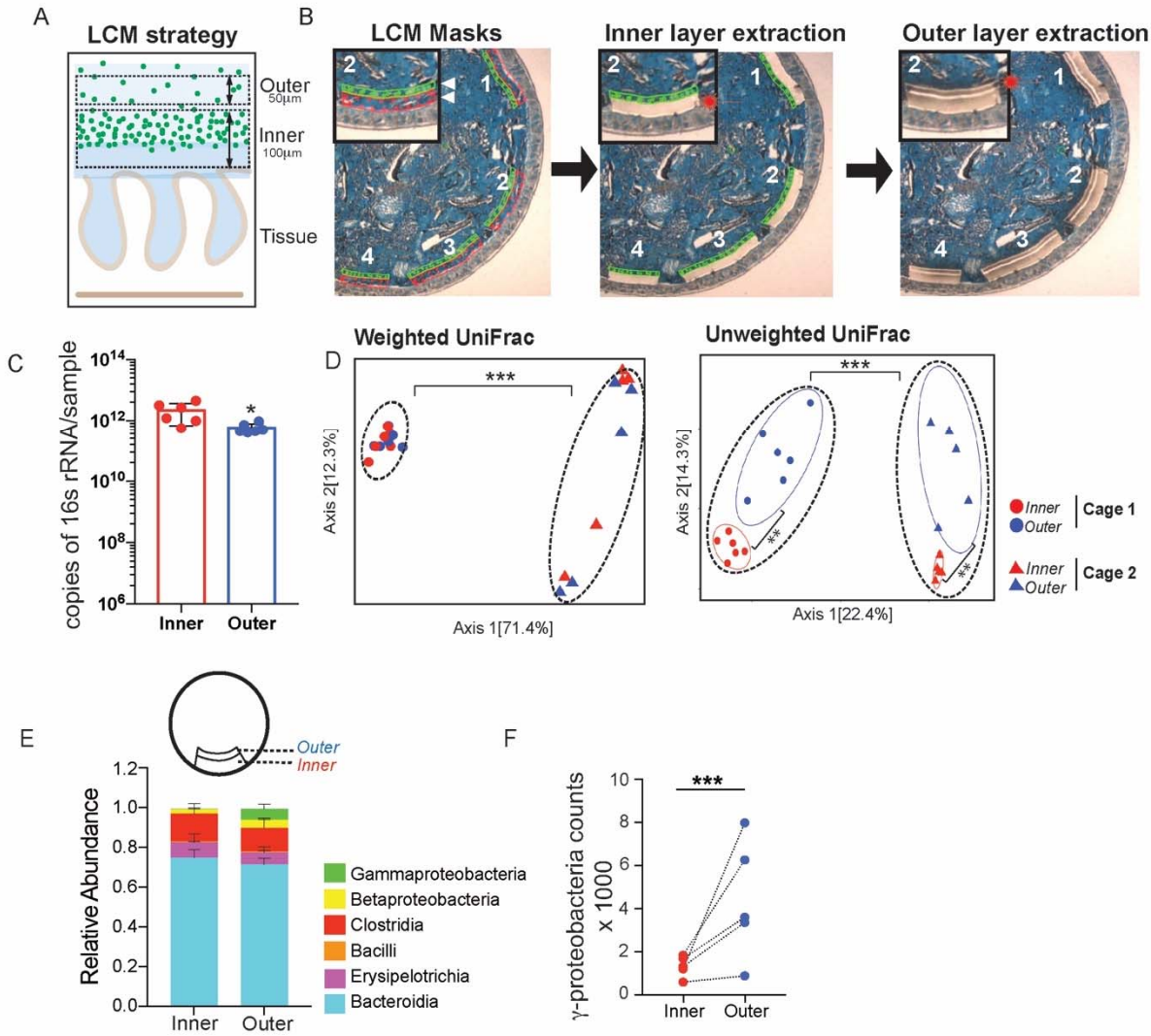

Figure 2. Mucus associated biofilm community is compositionally distinct from adjoining non-biofilm community.

A. Diagram of Laser capture microdissection (LCM) strategy for independently obtaining the inner biofilm community (1st 100-µm) and outer non-biofilm community (subsequent 50-µm) of the mucosal layer for 16S rRNA sequencing.

B. Images of colonic cross sections showing LCM masks of inner and outer communities followed by the independent extraction of each region separately in order to analyze regions separately.

C. Copy number of 16S rRNA per sample from inner and outer communities showing enough material is obtained for sequencing, with more copies in the inner biofilm (N=6). *$p < 0.05$ paired t-test.

D. Principal coordinates of analysis (PCoA) plots. Left: Weighted UniFrac shows most significant difference in microbial communities comes from cage effect, with no difference in location. Right: Unweighted UniFrac shows most significant difference in microbial communities comes from cage effect, but also the inner and outer communities are significantly different (N=11). **$p < 0.01$, ***$p < 0.001$ PERMANOVA.

E. Class level relative abundance of inner and outer communities (N=5).

F. Differential abundance of class Gammaproteobacteria, showing significantly more Gammaproteobacteria in the outer non-biofilm community (N=5, Log2 Fold Change=4.87, padj=1.39 x 10-7). ***$p < 0.001$ DESeq2.

Figure 3.

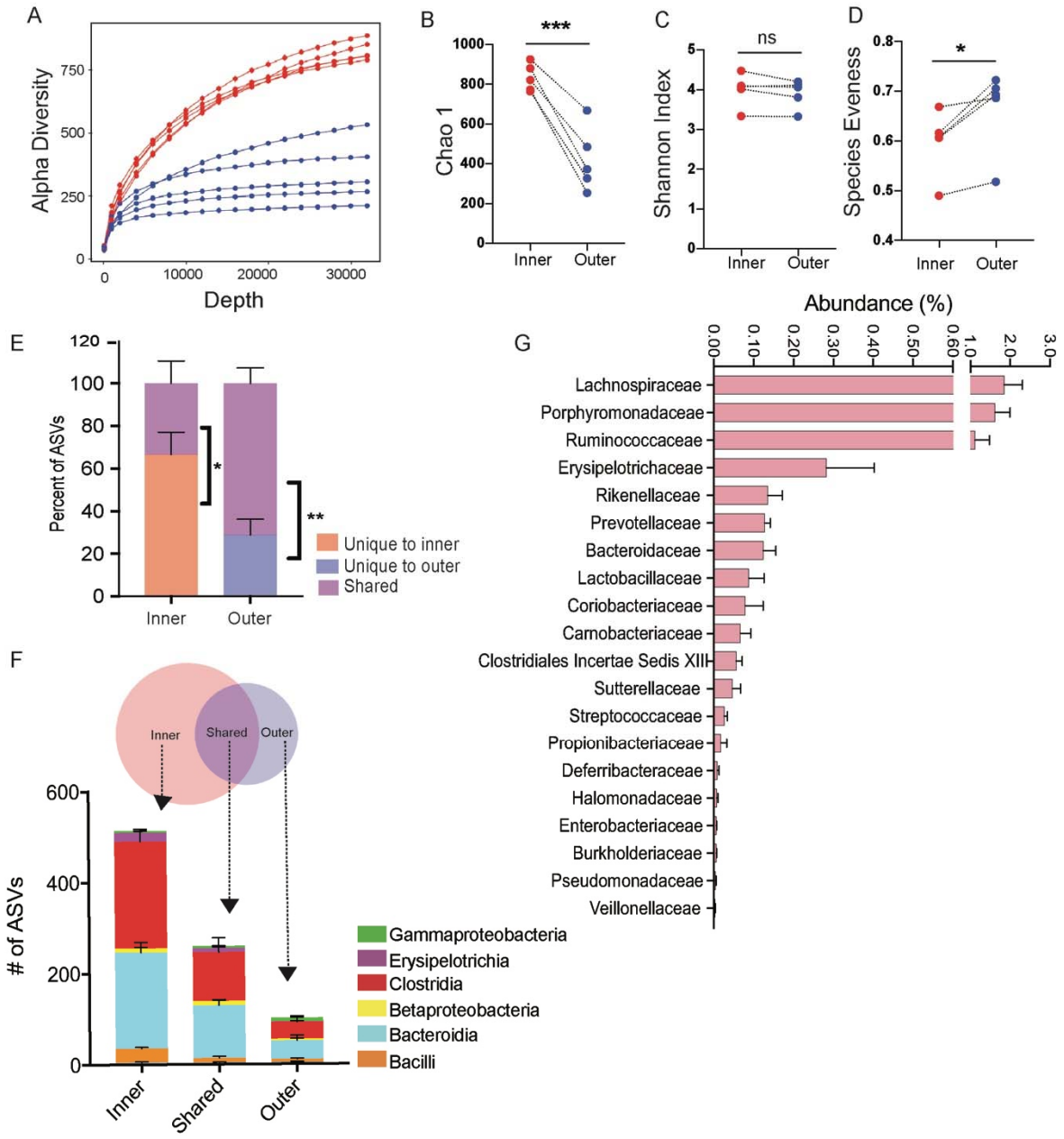

Figure 3. Biofilm community has significantly higher species richness due to presence of low abundance unique amplicon sequence variants (ASVs).

A. Alpha Rarefaction Curves plotting the number of unique amplicon sequence variants (ASVs) from inner biofilm (red) and outer non-biofilm communities (blue) showing more unique ASVs found in the inner biofilm community (N=5).

B. Chao1 diversity index showing significantly higher richness in the inner biofilm community (N=5). ***$p < 0.001$ paired t-test

C. Shannon diversity index showing no difference in Shannon diversity between inner and outer communities (N=5).

D. Pielou's Evenness index showing significantly higher evenness in the outer non-biofilm community (N=5). *$p < 0.05$ paired t-test

E. Proportion of ASVs found either unique to either region or shared within each mouse showing the inner biofilm maintains a large proportion of unique ASVs and the outer non-biofilm mostly consists of ASVs also found in the inner biofilm (N=5). *$p < 0.05$, **$p < 0.01$ paired t-test

F. Number of ASVs found either unique to either region or shared within each mouse condensed by class showing the increased richness in the inner biofilm is comprised of unique ASVs from classes Clostridia and Bacteroidia (N=5).

G. Abundance of unique ASVs in the inner biofilm of each mouse condensed by family to show the unique ASVs of the inner biofilm are at low abundance (N=5).

Figure 4

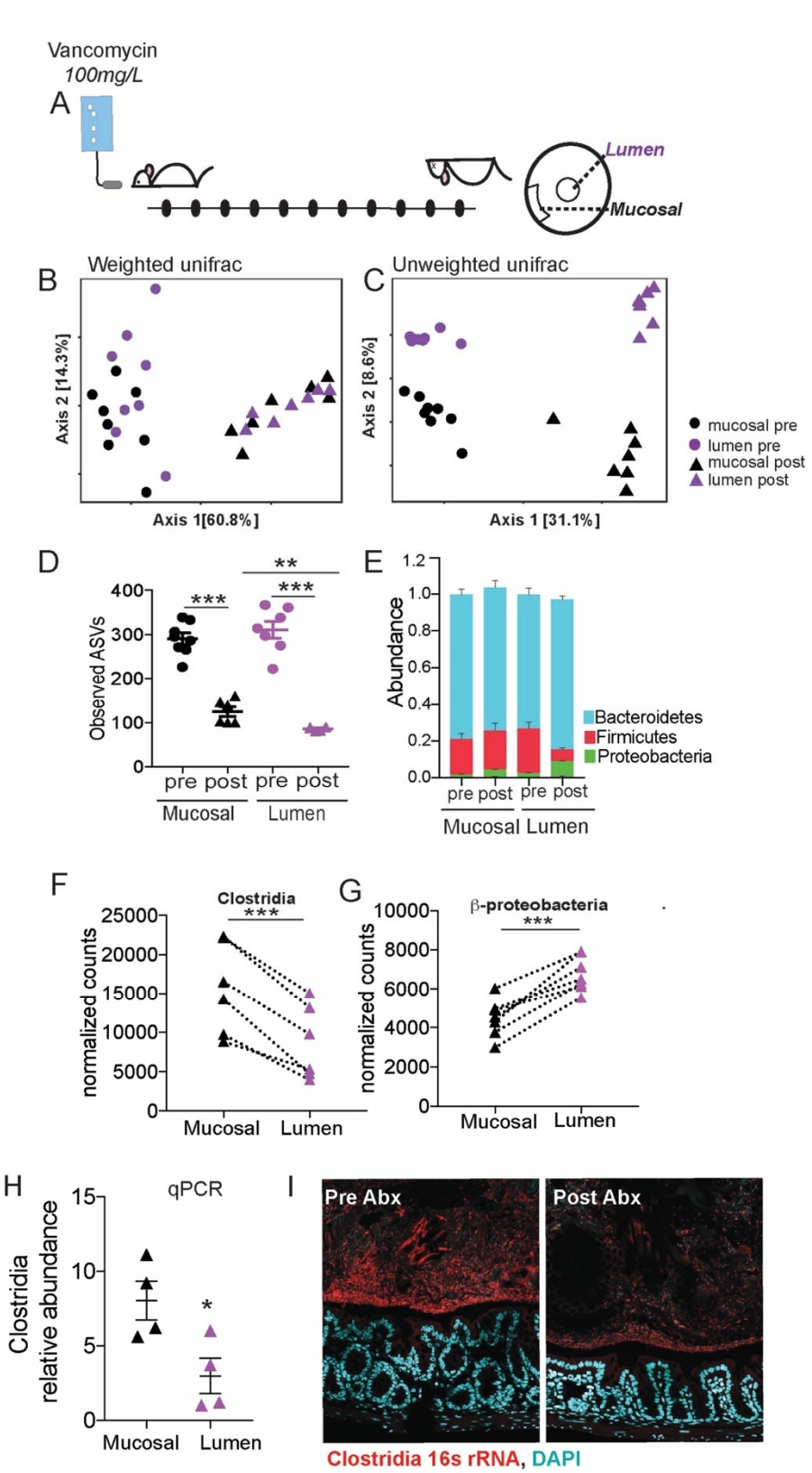
Vancomycin
100mg/L
A
Lumen
Mucosal
B
Weighted unifrac
Axis 2 [14.3%]
Axis 1[60.8%]
C
Unweighted unifrac
Axis 2 [8.6%]
Axis 1 [31.1%]
mucosal pre
lumen pre
mucosal post
lumen post
D
Observed ASVs
***
**
***
pre post pre post
Mucosal Lumen
E
Abundance
Bacteroidetes
Firmicutes
Proteobacteria
pre post pre post
Mucosal Lumen
F
Clostridia
***
normalized counts
Mucosal Lumen
G
β-proteobacteria
***
normalized counts
Mucosal Lumen
H
qPCR
Clostridia relative abundance
*
Mucosal Lumen
I
Pre Abx
Post Abx
Clostridia 16s rRNA, DAPI

Figure 4. Following antibiotics treatment biofilm community maintain higher species richness and is less prone to dysbiosis than luminal community.

A. Experimental design for comparing effects of antibiotics on spatially distinct regions of the gut microbiome. Provided mice water with 100mg/L of Vancomycin in drinking water. Sacrificed after 10 days of treatment.

B. Principal coordinates of analysis (PCoA) plot using weighted UniFrac distances shows both mucosal and luminal communities are significantly altered by antibiotic treatment (N=7 per group).

C. Principal coordinates of analysis (PCoA) plot using unweighted UniFrac distances shows both mucosal and luminal communities are significantly altered by antibiotic treatment (N=7 per group).

D. Number of unique ASVs found in each sample at rarefied depth of 39,464 reads (N=7 per group) showing a significant depletion in richness in both locations following antibiotic treatment (paired t-test) and the luminal community lost significantly more ASVs than the mucosal community following antibiotic treatment (unpaired t-test). **$p < 0.01$, *** $p < 0.001$.

E. Phylum-level relative abundance for pre- and post-antibiotic mucosal and luminal communities. (N=7 per group).

F. Differential abundance of class Clostridia, showing significantly more Clostridia in the mucosal community after antibiotic treatment (N=7 per group, Log2 Fold Change=1.33, padj=0.034). ***$p < 0.001$ DESeq2.

G. Differential abundance of class β-Proteobacteria, showing significantly more Clostridia in the mucosal community after antibiotic treatment (N=7 per group, Log2 Fold Change=0.59, padj=0.034). ***$p < 0.001$ DESeq2.

H. qPCR quantification of Clostridia relative abundance of mucosal and luminal communities after antibiotics, showing increased Clostridia in the mucosal community following treatment (N=4 per group). *$p < 0.05$ paired t-test.

I. FISH images of mucosal communities before and after Vancomycin treatment showing the greater prevalence of Clostridia (red) before treatment and the reduction after antibiotics, and the greater maintenance of Clostridia in the biofilm-like structure adjacent to the host epithelium (blue) following treatment.